Spinodal-assisted nucleation during symmetry-breaking phase transitions

Daniel A. Vega* and Leopoldo R. Gómez†
Department of Physics, Universidad Nacional del Sur-CONICET, Av L.N. Além 1253, 8000 Bahía Blanca, Argentina
(Received 28 October 2008; revised manuscript received 21 March 2009; published 29 May 2009)

The kinetics of spinodal-assisted crystallization in a region of the phase diagram where the dynamics is controlled by the critical slow down was studied by means of a Cahn-Hilliard model. The length-scale selectivity conducted by the spinodal process led to the formation of a filamentary network of density fluctuations that resemble the scarred states found in quantum-chaos systems. The present work reveals that the early structure of density fluctuations acts such as a precursor for crystallization and deeply affects the orientational and translational correlation between growing crystals. At deep quenches the network of fluctuations is deeply modified and the classical picture of spinodal decomposition is recovered.

DOI: 10.1103/PhysRevE.79.051607 PACS number(s): 64.60.Q−, 64.60.Bd, 64.70.dg, 64.70.Nd

I. INTRODUCTION

The processes of structure out of a homogeneous system undergoing a symmetry-breaking phase transition is an important phenomenon encountered in a large number of quite dissimilar areas such as condensed matter [1], particle physics, and cosmology [2]. One of the main mechanisms leading to phase separation in different systems is spinodal decomposition (SD). This process has been investigated in a wide number of systems such as inorganic glasses, polymers, metal alloys, liquid metal films, or colloidal systems. Differently from the nucleation and growth process, SD does not require large fluctuations to initiate the phase separation and it is characterized by the exponential growth of density fluctuations of a dominating wavelength entirely determined by the thermodynamic properties of the system [3], [4].

In the classical view of SD, at early times the wavelength selectivity gives rise to the well-known ring in the pattern of scattered radiation. In real space, the wavelength selectivity is visualized as a labyrinthic pattern of density fluctuations. As time proceeds, an array of domains with short-ranged order develops. The last stage kinetics of the SD process involves a coarsening toward the equilibrium of the coexisting phases [5–7].

Since most of the experimental approaches to study the process of SD are based in x-ray scattering techniques, the kinetics of ordering is naturally analyzed in the reciprocal Fourier space. Theoretically, most of the studies on SD have been focused in binary systems where the kinetics of phase separation can be well described through the classical Cahn-Hilliard approach.

Figure 1 illustrates the typical scattering functions associated to early and late stages of SD. When a binary blend is suddenly quenched into the unstable region of the phase diagram, at early times there is a strong length-scale selectivity that leads to the disordered pattern shown in Fig. 1. During this stage there an exponential amplification of the unstable modes. As time proceeds, the kinetic pathway toward equilibrium involves a coarsening process. During this process the main peak position of the scattering functions shifts toward the low-k region. Figure 1 also shows the typical scattering function of SD in off-critical systems with competing interactions. Although in this case there is sharper length-scale selectivity, the patterns are quite similar to those found in binary systems. As time proceeds the competing interactions lead to a pattern with a liquid-like order. In this case, long-range order can be achieved by the slow annihilation of topological defects.

Differently from the standard pictures of nucleation and growth or SD, experimental data on different systems also suggest an alternative pathway toward equilibrium involving a combination of both mechanisms [8–17].

Experimental and theoretical results on different polymeric systems clearly indicate spinodal kinetics before the emergence of the crystalline structure [8–11]. During the early stage of phase separation there is an induction time where density fluctuations of a given wavelength are con-

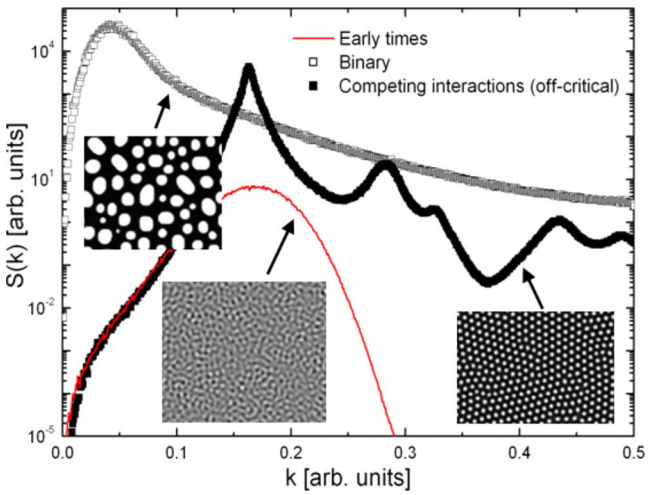

FIG. 1. (Color online) Circularly averaged scattering function $S(k)$ and patterns of the order parameter at short (line) and long times (symbols) for two different off-critical systems. The late-time behavior corresponds to binary (open symbols) and competing interactions systems (filled symbols). Although at short times there is strong length-scale selectivity in both systems, in the classical view of SD the late-time configuration involves the formation of growing domains via a coarsening process.

*dvega@criba.edu.ar
†lgomez@uns.edu.ar

tinuously amplified. Although most of the studies have been focused in the crystallization process of polymers and proteins [12], similar findings in systems where the nature of the interactions is completely different such as self-organized nanocrystalline alloys [13], Rayleigh–Bénard convection patterns [14,15], or thin-film dewetting [16,17], suggest the existence of an universal phenomenon where SD enhance the nucleation of the equilibrium structure. Another signature of universality is provided by experimental data on polymer crystallization and dewetting indicating the existence of correlations between growing domains [11], [16]. At present, neither the link between the density fluctuations and the precursors for crystallization nor the origin of such correlations has been clearly established.

Here we investigate the process of spinodal-assisted nucleation by means of a Cahn-Hilliard model [3], [7]. This is one of the simplest theoretical pictures to describe the process of symmetry-breaking phase transitions. Although this model does not contemplate any detailed information about the free energy, it has the great advantage of allowing to describe the universal mean-field response of a number of systems [18]. As compared with previous studies, here we focus our attention in the spinodal zone in the region close to the metastability limit, where both length-scale selectivity and critical slowing down allow us to identify the main features of the precursors for crystallization.

II. DYNAMICAL MODEL

In the neighborhood of the critical temperature, the free energy of a wide variety of systems with strong wavelength selectivity such as Langmuir films, block copolymers, magnetic garnets, or ferrofluids can be phenomenologically described by an order parameter free-energy functional of the form [18]:

$$F = \int d\mathbf{r}^3 \left[U(\psi) + \frac{D}{2}(\nabla\psi)^2 \right] + \frac{\beta}{2}\int\int d\mathbf{r}^3 d\mathbf{r}'^3 G(\mathbf{r}-\mathbf{r}')\psi(\mathbf{r})\psi(\mathbf{r}') \quad (1)$$

where $\psi(\mathbf{r})$ is the order parameter (OP) (e.g., local density or magnetization in block copolymers, or magnetic systems, respectively), $G(\mathbf{r})$ is a solution of $\nabla^2 G(\mathbf{r}) = -\delta(\mathbf{r})$ and $U(\psi) = -\frac{1}{2}\tau\psi^2 + \frac{1}{3}\nu\psi^3 + \frac{1}{4}\kappa\psi^4$. The parameters β, ν, κ, and D are phenomenological constants which can be computed from microscopic models [18] and τ provides a measurement of the depth of quench. In the spinodal region, $U(\psi)$ favors periodic profiles of well-defined wavelength and symmetry. The last term in Eq. (1) takes into account the long-range free-energy contribution [7], [18].

For a conserved order parameter, the relaxational dynamics can be described by the following Cahn-Hilliard equation:

$$\frac{\partial\psi}{\partial t} = M\nabla^2\left\{\frac{\delta F}{\delta\psi}\right\} \quad (2)$$

where M is a mobility coefficient. Eq. (2) leads to SD for $\tau > \tau_s = 2\sqrt{\beta D}$ being τ_s the spinodal temperature.

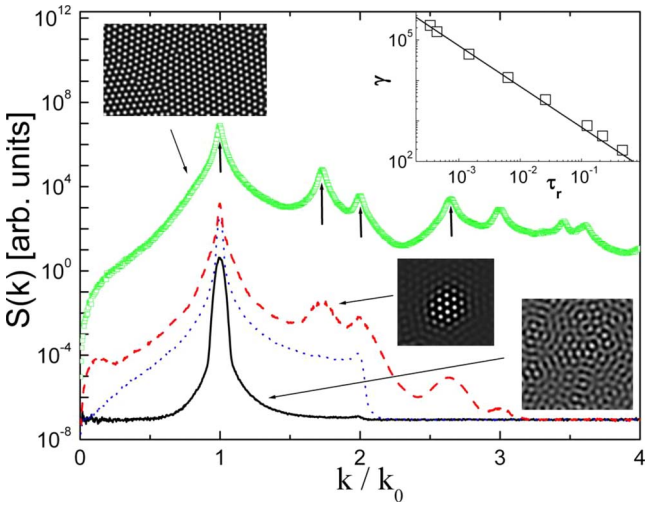

FIG. 2. (Color online) (a) Circularly averaged scattering function at different time scales $S(k)$ for $\tau_r = 10^{-3}$ at early [$\lambda(k_0)t = 5 \times 10^{-2}$ continuous line], intermediate [$\lambda(k_0)t = 2 \times 10^{-1}$ dotted line; $\lambda(k_0)t = 8.5 \times 10^{-1}$ dashed line] and long [$\lambda(k_0)t = 1$ symbols] times. The arrows highlight the positions of the main and higher-order reflections associated with the crystalline structure. The inset shows the induction period γ as a function of τ_r (symbols) and power-law fit (line).

Equation (2) was numerically solved with a random initial condition, in the hexagonal region ($\tau \gtrsim \tau_s$ and $\nu \neq 0$) for a two-dimensional system containing $\sim 2.5 \times 10^4$ disks. The mobility coefficient was set at $M = 1$ and the phenomenological parameters in the free energy were fixed at $\nu = 0.023$, $\kappa = 0.38$, $\beta = 0.03$, and $D = 0.3$. The noise term was ignored except to include it as providing initial randomness in the system. We have also conducted studies that include thermal fluctuations and have confirmed that fluctuations renormalize the depth of quench increasing the pseudonucleation rate. For more details about the scheme of resolution of Eq. (2) see Ref. [7].

III. PRETRANSITIONAL STATE

Shortly after the quench the order parameter is small ($\psi \sim 0$) and the stability of the system can be analyzed by considering the order parameter as a linear superposition of functions with the form: $\phi_{\mathbf{k}}(\mathbf{r},t) = \exp[i\mathbf{k}\cdot\mathbf{r} + \lambda(k)t]$, where $\lambda(k) = -Dk^4 + \tau k^2 - \beta$ [3]. Then, there is only a bounded range of high temperature unstable modes that can grow ($\lambda(k) > 0$). From the narrow range of these growing modes, there is one which propagates faster ($k_0^2 = \tau/D$) and rapidly selects a length scale in the system. The strong k selectivity can be clearly observed through the circularly averaged scattering function $S(k)$ shown in Fig. 2, where the main peak position defines a dominating length-scale a: $a \sim 1/k_0$. Here $S(k)$ was determined as $S(k) = \langle \tilde{\psi}(\mathbf{k})\tilde{\psi}(\mathbf{k})^* \rangle$, where $\tilde{\psi}(\mathbf{k})$ represents the Fourier transform of the order parameter.

IV. RANDOM SUPERPOSITION OF MODES

At early times $\psi(\mathbf{r},t)$ can be expressed as: $\psi(\mathbf{r},t) \sim \int d\Omega \psi_{\mathbf{k}}\phi_{\mathbf{k}}(\mathbf{r},t)$ where $\psi_{\mathbf{k}}$ is the initial amplitude of the $\mathbf{k}$

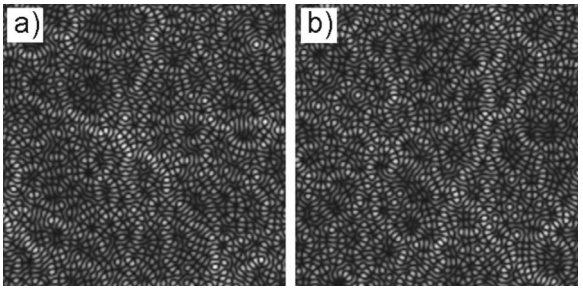

FIG. 3. (a) Pattern corresponding to the absolute value of a function obtained as a random superposition of 5000 sinusoidal waves of fixed k. (b) $|\psi(\mathbf{r})|$ at early times $[\lambda(k_0)t=5\times10^{-2}$, $\tau_r=10^{-3}]$. Regions where the order parameter is larger appear lighter than the average. Note the similarities between both patterns.

mode, that is, $\psi(\mathbf{r},t)$ can be represented as a random superposition of sinusoidal modes.

Figure 3(a) shows a typical pattern obtained as a random superposition of sinusoidal waves of constant k. Contrary to physical intuition, a superposition of modes with nearly constant k and random amplitudes, phases, and directions does not result in a distribution of amplitudes that resembles an unstructured speckle-like pattern, but exhibits a filamentary network of quasilinear density fluctuations [19]. These ridged structures, dubbed scarlets by Eric Heller [20], are a general wave phenomenon and are present in systems where the dynamics is represented as a random superposition of modes such as quantum billiards [20], [21] or surface-wave patterns [22].

Although quite common in the jargon of quantum chaos, the influences of these ridged structures have been never taken into account in the process of phase separation. As we show below, this pretransition ridged state in the density fluctuations not only controls the formation of well-ordered domains during SD but also introduce long-range correlations between the precursors.

Even though the filamentary structure of density fluctuations is completely "hidden" in the ring of scattered radiation, they can be clearly identified in real space. Figure 3(b) shows the pattern of $|\psi(\mathbf{r})|$ at the initial stage of SD $[t\ll\lambda(k_0)^{-1}]$. Note the similarities with the pattern obtained via the random superposition of sinusoidal waves (Fig. 3(a)).

The real-space two-point correlation function defined as $C(\mathbf{r})=\int d\mathbf{r}'\psi(\mathbf{r}')\psi(\mathbf{r}+\mathbf{r}')$ for an order parameter given by a random superposition of modes of constant k becomes $C(r)\sim J_0(k_0r)$, where J_0 is the Bessel function of zero order [19], [23].

Figure 4 shows $C(r)$ for the early process of SD at two different temperatures. At temperatures nearly close to the spinodal $S(k)$ is sharply peaked around k_0 and $C(r)$ behaves such as a Bessel function decaying asymptotically as $C(r)\sim1/\sqrt{k_0r}$. However, as the temperature is reduced the width of the ring of unstable modes becomes thicker (see inset of Fig. 4) and asymptotically $C(r)$ behaves such as $C(r)\sim\exp(-r/\xi_C)$, defining in this way a characteristic length scale ξ_C for the decaying of the density correlations. The inset of Fig. 4 clearly shows the profound effect that the mode selectivity has on the network of density fluctuations.

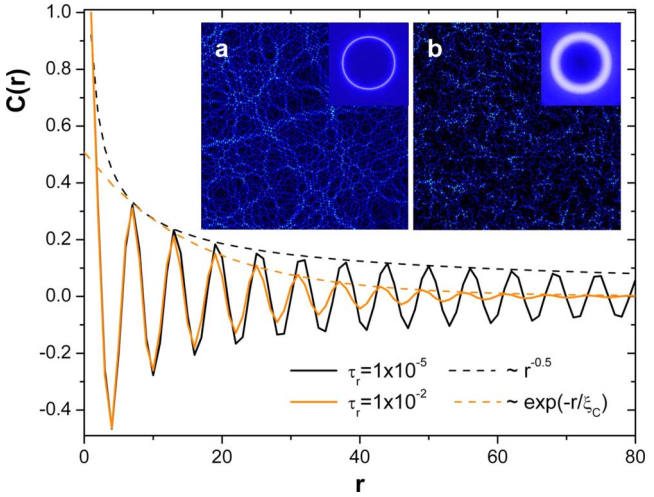

FIG. 4. (Color online) Two points correlation function $C(r)$ as a function of the distance r at two different reduced temperatures (continuous lines) and asymptotic behavior (dashed lines). The insets indicate the real ($|\psi(\mathbf{r})|$) and Fourier-space ($S(k)$) representation of for $\tau_r=10^{-5}$ (a) and $\tau_r=10^{-2}$ (b). Note the influence of the temperature in the early network of density fluctuations.

V. SPINODAL-ASSISTED NUCLEATION

As a consequence of the continuous amplification of the order parameter, as time proceeds, the nonquadratic terms in $U(\psi)$ acquires a larger relative importance and nonlinear dynamics comes into play. However, due to the presence of the ridged structure, the effect of nonlinearities is not homogeneous. Although there is a continuous amplification of $\psi(\mathbf{r})$ everywhere, it amplifies faster at regions with initially larger fluctuations, i.e., ridges. Because the nonlinearities define the crystalline symmetry, preferentially amplified ridges trigger the nucleation of well-ordered domains that rapidly propagates throughout the system.

Figure 2 also includes the circularly averaged structure factor at intermediate and long times. As time proceeds, there is a regeneration of modes and the scattering function shows an increase in the main peak intensity and well-defined higher-order peaks at the positions expected for the crystalline structure [6]. Through $S(k)$, it is possible also to note the low k-mode regeneration mainly associated to the contribution of the form factor [1] of the growing domains.

In Fig. 5 we show the complete process of spinodal-assisted nucleation as seen through the order parameter. At early times it is observed that in the branching points of the network of ridges trigger the nonlinear terms in the free-energy functional (Fig. 5(a)). Then, a small seed of the equilibrium phase is created at these points (Fig. 5(b)). While in the interior of these seeds there is a continuous amplification of the order parameter until saturation, the front of the growing grains propagates through the system at a constant temperature-dependant velocity (Fig. 5(c)). Then, the collision between the different domains leads to a polycrystalline structure (Fig. 5(d)) with an average domain size controlled by the temperature.

Note that instead of a pattern with a short-ranged correlation length, as expected for SD, here we observe the propa-

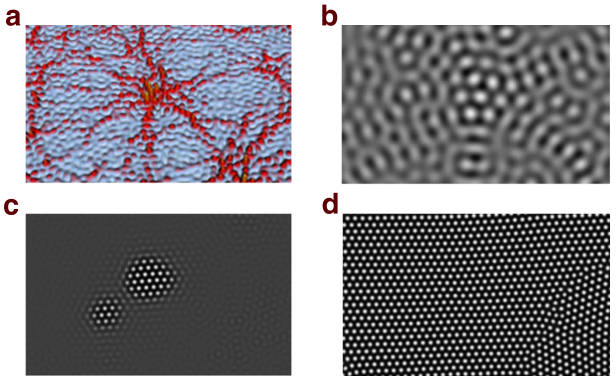

FIG. 5. (Color online) Pseudonucleation of the hexagonal phase triggered by the fast amplification of the branching points of the early network of scars at short time $[\lambda(k_0)t=2\times10^{-1}]$ as seen though $\psi(r)^2$ (panel a) and $\psi(r)$ (panel b). Bottom: (c) Propagation $[\lambda(k_0)t=8.5\times10^{-1}]$ and (d) collision of domains $[\lambda(k_0)t=1]$. Note the excellent orientational and translational order inside each domain.

gation and collision of coherent domains with an excellent translational and orientational order. Then, even though the process of phase separation is conducted in the spinodal region, the inhomogeneities produced by the random superposition of modes provide the seeds for crystallization. Since the amplification factor $\lambda(k_0)$ goes to zero at τ_s $[\lambda(k_0)\sim\tau-\tau_s]$, the induction period γ prior to the emergence of ordered domains is controlled by the so-called critical slow down (see the inset of Fig. 2), i.e., $\gamma\sim\tau_r^{-1}$, where $\tau_r=\tau/\tau_s-1$.

In order to unveil the correlation between propagating crystals and the underlying ridges, we use the Minkowski measurement. As shown by Herminghaus *et al.*, this method is very sensitive to spatial correlations in the distribution of the initial ensemble of pseudonucleation seeds [16]. In Fig. 6, we plotted one of the Minkowski measurements (normalized total area A of the pattern) as a function of the disk radius, r. In contrast with a random distribution, our data show substantial deviations confirming that the domains are not generated by a random process. The presence of the correlations in the spatial distribution of the grain positions demonstrate is inherited to the specific correlations imposed by the spinodal process. The existence of the correlations can be also observed in real space in the inset of Fig. 6 where the ridges trigger the formation of hexagonally-ordered crystals along a preferential direction.

Another quantitative analysis to detect the presence of correlations can be made by comparing the average crystal size and the length-scale ξ_c associated to the asymptotic behavior of $C(r)$. The average crystal size can be estimated through the full width at half maximum of the main peak of $S(k)$: $\xi_T\sim\delta S_{HW}(t)^{-1}$ [6,7]. In Fig. 7 we plot ξ_T and ξ_C as a function of the reduced temperature τ_r. We can observe that both correlation lengths scale with τ_r according to a power-law consistent with $\xi_T\sim\xi_C\sim\tau_r^{-1/5}$ indicating the existence of a strong correlation between early and late structures.

In addition to the positional correlation between growing crystals observed in Fig. 6, the early network of density fluctuations also induce orientational correlations between the

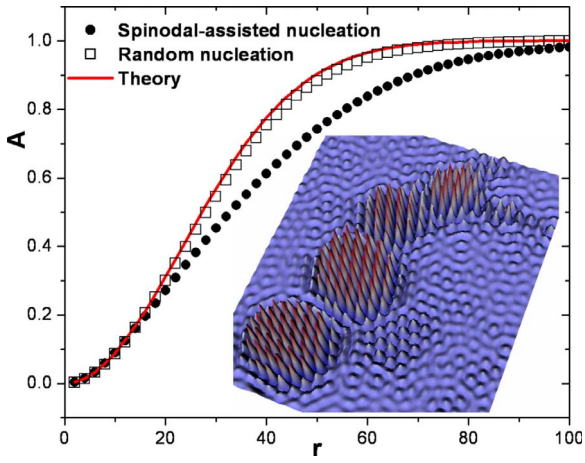

FIG. 6. (Color online) Minkowski measurement A as a function of the disk radius r. Continuous line and squares represent theoretical and simulated data for a random distribution of nuclei, respectively. Circles correspond to the spinodal-assisted nucleation mechanism studied here. The inset clearly shows the formation of correlated-hexagonal crystals.

crystals. Since different precursors for crystallization can be located along a given ridge, a preferential direction for the orientation of the crystals is clearly defined during the induction period $[t<\lambda(k_0)^{-1}]$. To emphasize the differences between translational and the orientational correlations, in Fig. 7 we also shows the orientational correlation length ξ_6 measured at long times.

To determine ξ_6 at different temperatures the orientational correlation function $g_6(r)$ was obtained as $g_6(r)=\langle\exp\{6i[\theta(r)-\theta(r')]\}\rangle$. Here $\theta(\mathbf{r})$ is the local orientation at position $\mathbf{r}$. To determine $g_6(r)$ a standard procedure was implemented to identify the position of each disk in the hexagonal pattern [7]. The local interdisks bond orientation in

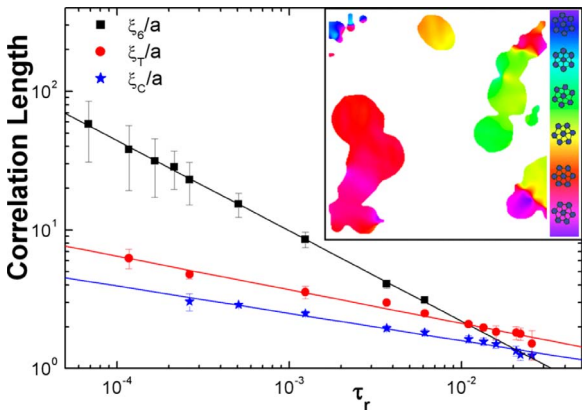

FIG. 7. (Color online) Correlation lengths as a function of τ_r (symbols indicated in the figure). The inset shows the local orientation of growing crystals at a shallow quench and intermediate times $[\tau_r=10^{-3}, \lambda(k_0)t=8.5\times10^{-1}]$. The different colors (gray intensity) indicate the local orientation of the hexagonal lattice and also provide a measure of the average grain size. The strong orientational correlation between growing domains is induced by the early networks of density fluctuations. Color (gray) scale and lattice orientation indicated on the right.

the hexagonal phase was determined in real space by a Delaunay triangulation through the center of the disks. The color (gray) key employed to identify the domains in Fig. 7 indicates the orientational field over the range $[0,\pi/3]$, as appropriate for a sixfold-symmetric structure. Then, ξ_6 was determined by approximating the circularly averaged orientational correlation function $g_6(r)$ with a single exponential: $g_6(r)\sim\exp(-r/\xi_6)$.

We found that the dependence of ξ_6 with τ_r is also consistent with a power-law behavior: $\xi_6\sim\tau_r^{-2/3}$. As compared with ξ_T and ξ_C, ξ_6 is more strongly dependant on τ_r, indicating the existence of orientational correlations between growing crystals. Such correlation can be observed in the inset of Fig. 7, where the local orientation of the growing crystals has been identified through the color (gray) map. Note that the orientation of several near-neighbor propagating grains is strongly correlated. As previously discussed these correlations are provided by the early structure of density fluctuations.

Although at shallow quenches the orientational correlation length is about one order of magnitude larger that ξ_T, by increasing the depth of quench beyond $\tau_r\sim 10^{-2}$, the domain size becomes comparable to one-lattice constant ($\xi_6\sim\xi_T\sim a$). Below this temperature, nonlinearities are triggered uniformly throughout the system, the formation of ordered domains with long-range order is inhibited and the process of SD reduces to the classical picture.

It is interesting to note that the experimental data of Heeley *et al.* for polymer crystallization show a different kinetic regime for shallow ($\tau_r=0.004$) and deep quenches ($\tau_r=0.05$) [9]. Although in our case the wavelength selectivity could be stronger that in polymer crystallization, the similarity in the values of τ_r separating both regimes is quite surprising. Finally, we may also note that the existence of correlations may explain the departures from Avrami's kinetics found during polymer crystallization [9].

VI. CONCLUDING REMARKS

The frustration of the order parameter to reach equilibrium at the interfaces of colliding domains is often visible through topological defects, which mediate between different degenerated ground states [6,7]. During the last years it has been a great effort to elucidate the mechanisms leading to the formation and features of topological defects and different condensed matter systems such as liquid Helium ^{3}He or liquid crystals have been employed to test theoretical scenarios [2], [24–27]. Since here the domains propagate free of orientational or translational distortions, the totality of the orientational defects are condensed along domain boundaries and its density is entirely controlled by the reduced temperature in qualitative agreement with Kibble's picture for cosmological phase transitions [24], [26]. However, here the early network of density fluctuations introduce a strong orientational correlation between propagating domains, which reduces the density of trapped topological defects predicted by Kibble's picture [24].

Finally, since the underlying mechanism of phase separation described here is general to a broad class of systems where the early kinetics is controlled by a dominating length-scale, this work provides unambiguous insight into the dynamics of symmetry-breaking phase transitions and shed light on the early stage of ordering leading to crystallization. Our work clearly shows that contrary to the current belief, it is possible to obtain large and perfectly ordered crystals during continuous symmetry-breaking phase transitions. It is hoped that this work will stimulate experimental research to study the process of spinodal-assisted nucleation.

ACKNOWLEDGMENTS

We gratefully acknowledge R. A. Register, S. T. Milner, P. M. Chaikin, W. Soboyejo and D. A. Huse for stimulating discussions. This work was supported by the National Research Council of Argentina (CONICET), and the USAMI program of the National Science Foundation through Princeton University.

[1] P. M. Chaikin and T. C. Lubensky, *Principles of Condensed Matter Physics* (Cambridge Univ. Press, Cambridge, 1995).
[2] *Proceedings of the NATO-ASI on topological defects and non-equilibrium dynamics of symmetry-breaking phase transitions edited by* Y. Bunkov and H. Godfrin (Kluwer, Dordrecht) (2000).
[3] J. W. Cahn, J. Chem. Phys. **42**, 93 (1965).
[4] P. G. Debenedetti, *Metastable Liquids: Concepts and Principles* (Princeton Univ. Press, Princeton, 1996).
[5] A. J. Bray, Adv. Phys. **43**, 357 (1994).
[6] D. A. Vega, C. K. Harrison, D. E. Angelescu, M. L. Trawick, D. A. Huse, P. M. Chaikin, and R. A. Register, Phys. Rev. E **71**, 061803 (2005).
[7] L. R. Gómez, E. M. Valles, and D. A. Vega, Phys. Rev. Lett. **97**, 188302 (2006).
[8] P. D. Olmsted, W. C. K. Poon, T. C. B. McLeish, N. J. Terrill, and A. J. Ryan, Phys. Rev. Lett. **81**, 373 (1998).
[9] E. L. Heeley, A. V. Maidens, P. D. Olmsted, W. Bras, I. P. Dolbnya, J. P. A. Fairclough, N. J. Terrill, and A. J. Ryan, Macromolecules **36**, 3656 (2003).
[10] M. Muthukumar, Lect. Notes Phys. **714**, 1 (2007).
[11] R. H. Gee, N. Lacevic, and L. E. Fried, Nat. Mater. **5**, 39 (2006).
[12] P. R. ten Wolde and D. Frenkel. Science **277**, 1975 (1997).
[13] J. Li, Appl. Phys. Lett. **90**, 041913 (2007).
[14] E. Bodenschatz, J. R. de Bruyn, G. Ahlers, and D. S. Cannell, Phys. Rev. Lett. **67**, 3078 (1991).
[15] E. Bodenschatz, D. S. Cannell, J. R. de Bruyn, R. Ecke, Y. –C. Hu, K. Lerman, and G. Ahlers, Physica D **61**, 77 (1992).
[16] S. Herminghaus, K. Jacobs, K. Mecke, J. Bischof, A. Fery, M. Ibn-Elhaj, and S. Schlagowski, Science **282**, 916 (1998).
[17] U. Thiele, M. G. Velarde, and K. Neuffer, Phys. Rev. Lett. **87**,

016104 (2001).
[18] M. Seul and D. Andelman, Science **267**, 476 (1995).
[19] P. O'Connor, J. Gehlen, and E. J. Heller, Phys. Rev. Lett. **58**, 1296 (1987).
[20] E. J. Heller, Phys. Rev. Lett. **53**, 1515 (1984).
[21] P. B. Wilkinson, T. M. Fromhold, L. Eaves, F. W. Sheard, N. Miura, and T. Takamasu, Nature (London) **380**, 608 (1996).
[22] A. Kudrolli, M. C. Abraham, and J. P. Gollub, Phys. Rev. E **63**, 026208 (2001).
[23] W. Klein, Phys. Rev. Lett. **65**, 1462 (1990).
[24] T. W. B. Kibble, J. Phys. A **9**, 1387 (1976).
[25] W. H. Zurek, Nature (London) **317**, 505 (1985).
[26] W. H. Zurek, Nature (London) **382**, 296 (1996).
[27] C. Bauerle, M. Yu, S. N. Fisher, H. Godfrin, and G. R. Pickett, Nature (London) **382**, 332 (1996).